Analysis of the land surface heterogeneity and its impact on atmospheric variables and the aerodynamic and thermodynamic roughness lengths

Article *in* Journal of Geophysical Research Atmospheres · April 2008

DOI: 10.1029/2007JD009124 · Source: OAI

4 authors:

Yaoming Ma
Chinese Academy of Sciences
202 PUBLICATIONS **3,761** CITATIONS
SEE PROFILE

Massimo Menenti
Delft University of Technology
441 PUBLICATIONS **8,354** CITATIONS
SEE PROFILE

Reinder Auke Feddes
Wageningen University & Research
147 PUBLICATIONS **8,706** CITATIONS
SEE PROFILE

Jiemin Wang
Northwest Institute of Eco-Environment and Resources (NIEER), Chinese Academy of…
91 PUBLICATIONS **2,218** CITATIONS
SEE PROFILE

JOURNAL OF GEOPHYSICAL RESEARCH, VOL. 113, D08113, doi:10.1029/2007JD009124, 2008

Analysis of the land surface heterogeneity and its impact on atmospheric variables and the aerodynamic and thermodynamic roughness lengths

Yaoming Ma,[1,2,3] Massimo Menenti,[4] Reinder Feddes,[5] and Jiemin Wang[3]

Received 3 July 2007; revised 21 October 2007; accepted 15 January 2008; published 24 April 2008.

[1] The land surface heterogeneity has a very significant impact on atmospheric variables (air temperature T_a, wind speed u, and humidity q), the aerodynamic roughness length z_{0m}, thermodynamic roughness length z_{0h}, and the excess resistance to heat transfer kB^{-1}. First, in this study the land surface heterogeneity has been documented through the comparison of surface reflectance r_0, surface temperature T_0, net radiation flux R_n, and sensible heat flux H partitioning over the different land cover types in the experimental areas of the Global Energy and Water Cycle Experiment (GEWEX) Asian Monsoon Experiment on the Tibetan Plateau (GAME/Tibet), the Coordinated Enhanced Observing Period (CEOP) Asia-Australia Monsoon Project on the Tibetan Plateau (CAMP/Tibet), the Heihe Basin Field Experiment (HEIFE), the Arid Environment Comprehensive Monitoring Plan, 95 (AECMP'95), and the Dun Huang Experiment (DHEX). The results show that the surface heterogeneity was very significant in the areas of the HEIFE, the AECMP'95, and the DHEX and that it was less significant in the areas of CAMP/Tibet and GAME/Tibet. Second, the vertical profiles of T_a, u, and q in the near-surface layer and above the blending height z_b have been analyzed using the atmospheric boundary layer (ABL) tower data, radiosonde data, and tethered balloon data observed during the HEIFE, the DHEX, and the CAMP/Tibet. The results show that the land surface heterogeneity leads in the near-surface layer to different vertical profiles of u, T_a, and q overlying the surfaces of the Gobi and the oasis in the areas of the HEIFE and DHEX. The values of u, T_a, and q become well mixed above a height of about 300 m at the HEIFE and 150 m at the DHEX. z_{0m}, z_{0h}, and kB^{-1} over the different land surfaces have also been determined in this study. The results show that the land surface heterogeneity leads to different aerodynamic and thermodynamic parameters over the areas of the HEIFE, the AECMP'95, and the GAME/Tibet.

Citation: Ma, Y., M. Menenti, R. Feddes, and J. Wang (2008), Analysis of the land surface heterogeneity and its impact on atmospheric variables and the aerodynamic and thermodynamic roughness lengths, *J. Geophys. Res.*, *113*, D08113, doi:10.1029/2007JD009124.

1. Introduction

[2] The land surface in the experimental areas of the Global Energy and Water Cycle Experiment (GEWEX) Asian Monsoon Experiment on the Tibetan Plateau (GAME/Tibet), the Coordinated Enhanced Observing Period (CEOP) Asia-Australia Monsoon Project on the Tibetan Plateau (CAMP/Tibet), the Heihe Basin Field Experiment (HEIFE), the Arid Environment Comprehensive Monitoring Plan, 95 (AECMP'95), and the Dun Huang Experiment (DHEX) is heterogeneous [*Ma et al.*, 2002, 2003a, 2003b, 2004]. This results in the heterogeneity of the energy partitioning at the surface, and further more, may result in the different structure of the convective atmospheric boundary layer (CABL) near the land surface. In this paper the land surface heterogeneity will be documented through the evaluation of spatial patterns of surface reflectance r_0, surface temperature T_0, net radiation flux R_n, and sensible heat flux H partitioning over the different land cover types in the experimental areas.

[3] The airflow and state over a heterogeneous land surface is influenced by surface heterogeneity, and it leads to spatial variability in the ABL state near the land surface. In the surface layer (SL) this results in different vertical profiles of air temperature T_a (or potential temperature θ),

[1]Institute of Tibetan Plateau Research, Chinese Academy of Sciences, Beijing, China.
[2]School of Geography and Remote Sensing, Beijing Normal University, Beijing, China.
[3]Cold and Arid Regions Environmental and Engineering Research Institute, Chinese Academy of Sciences, Lanzhou, China.
[4]Laboratoire des Sciences de l'Image, de l'Informatique et de la Télédétection, Université Louis Pasteur, Strasbourg, France.
[5]Department of Environmental Sciences, Wageningen University, Wageningen, Netherlands.

0148-0227/08/2007JD009124$09.00

wind speed u, and humidity q in response to changes in land surface properties. But the development of CABL tends to smooth out the at-surface variability at the "blending height," where atmospheric characteristics such as θ, u, and q become spatially uniform [*Wieringa*, 1986; *Mason*, 1988; *Claussen*, 1990, 1991]. The different vertical profiles of T_a, u, and q in the near-surface layer and above the blending height z_b will also be analyzed using the atmospheric boundary layer (ABL) tower data, radiosonde data, and tethered balloon data in this paper.

[4] The land surface heterogeneity leads to differences in the aerodynamic roughness length z_{0m}, the thermodynamic roughness length z_{0h}, and the excess resistance to heat transfer kB^{-1} over the different land surfaces. These near-surface boundary layer parameters over the different land surfaces will also be determined in this paper.

2. Land Surface Heterogeneity and Its Influences on the Overlying Surface Layer and Atmospheric Boundary Layer

[5] The land surface condition and the sites layout during the HEIFE, the CAMP/Tibet, and the DHEX are shown in Figure 1. The land surface heterogeneity and its influences on the overlying atmospheric layer over the different land surfaces of the HEIFE, the CAMP/Tibet, and the DHEX will be documented in this section by using the surface and ABL observational data in these experiments.

2.1. Diurnal Variation of Surface Reflectance, Surface Temperature, and Surface Heat Fluxes Over Heterogeneous Land Surfaces

[6] Figure 2 gives the diurnal variation of r_0, T_0, R_n and H over the oasis and the Gobi desert in the HEIFE area on 9 July 1991. The diurnal variations of r_0, T_0, R_n, and H over the CAMP/Tibet area in the months January, June, and August are shown in Figure 3. All the curves were obtained under clear-sky conditions. In Figures 2 and 3, T_0 was measured by an infrared radiometer, and r_0 was calculated from

$$r_0 = \frac{K_\uparrow}{K_\downarrow} \quad (-), \tag{1}$$

where $K_\downarrow$ (W m^{-2}) and $K_\uparrow$ (W m^{-2}) are the measured downward and upward short-wave radiation fluxes, respectively. R_n (W m^{-2}) in Figures 1 and 2 was calculated from

$$R_n = K_\downarrow - K_\uparrow + L_\downarrow - L_\uparrow \quad (\text{W m}^{-2}), \tag{2}$$

where $L_\downarrow$ (W m^{-2}) and $L_\uparrow$ (W m^{-2}) are the measured downward and upward long-wave radiation fluxes, respectively. H (W m^{-2}) in Figures 2 and 3 was calculated from the ABL tower data, which is

$$H = \rho c_p C_{HN}(u_{z2} - u_{z1})(T_{z2} - T_{z1}) \quad (\text{W m}^{-2}), \tag{3}$$

where ρ is air density, c_p is air specific heat at constant pressure, u_{z1} and u_{z2} are the wind speed at heights z_1 and z_2, respectively, and T_{z1} and T_{z2} are air temperature at the height z_1 and z_2, respectively. C_{HN} denotes the bulk transfer coefficient in the neutral state:

$$C_{HN} = \frac{k^2}{[\ln(z/z_{0m})]^2} \quad (-), \tag{4}$$

where k is Von Karman constant and z is the reference height.

[7] The following can be concluded:

[8] 1. The surface heterogeneity resulted in different values of r_0, T_0, R_n and H over the HEIFE area. The values of r_0, T_0 and H over the oasis (Linze station in Figure 1a) surface are much lower than those over the Gobi desert surfaces. R_n over the oasis is much higher than that over the Gobi and desert owing to its lower r_0 and lower T_0. The values of r_0, T_0, R_n and H in the Gobi zone and the desert zone are different, but the differences are not large.

[9] 2. Surface heterogeneity was observed at the stations in the CAMP/Tibet area: the MS3478 station has a relatively high vegetation fractional cover, while BJ and D105 have sparse vegetation covers. The land surface properties at the stations D105, MS3478, and BJ in the CAMP/Tibet are different; that is, r_0 is lower and R_n is higher over the MS3478 station. But the differences are not as large as those between oasis and desert; that is, surface heterogeneity is not very large in the CAMP/Tibet area as compared to that in the HEIFE area.

[10] 3. The intermonthly variations of r_0, T_0, R_n and H over the CAMP/Tibet area are very clear: T_0, R_n in summer (June and August) are higher than in winter (January), and r_0 and H in summer (June and August) are lower than in winter (January). The reason is that in summer the land surface is wet and the grass grows, and in winter the surface is covered by snow and ice and the grass is dry.

2.2. Influences of Surface Heterogeneity on the Overlying Convective Atmospheric Boundary Layer

[11] In order to show the influences of land surface heterogeneity on the overlying CABL, the vertical profiles of T_a, u, and q will be shown in this section.

[12] Figure 4 shows the vertical profiles of u, T_a, and q over the very different surfaces of the Gobi and the oasis (Linze station in Figure 1a) of the HEIFE area. Data used in Figure 4a were measured at an ABL tower, and the ones shown in Figure 4b were measured by means of a Tethered balloon. Figure 5 gives the vertical profiles of u, T_a, and q over the Gobi desert and the oasis (PAM station in Figure 1c) of the DHEX as measured by means of radio soundings (oasis) and Tethered balloon (Gobi), respectively. The vertical profiles of u, T_a, and q observed from the radiosonde system at the BJ station of the CAMP/Tibet are shown in Figure 6. The results show the following:

[13] 1. Owing to the different surface properties, the vertical profiles of u, T_a, and q overlying the surfaces of the Gobi and the oasis (Linze station in Figure 1a) in the HEIFE area are very different in the near-surface layer. The values of u and T_a below a height of about 300 m over the Gobi surface are higher than those over the oasis; q over the Gobi surface is lower than that over the oasis. The values of u, T_a, and q become almost the same at (and

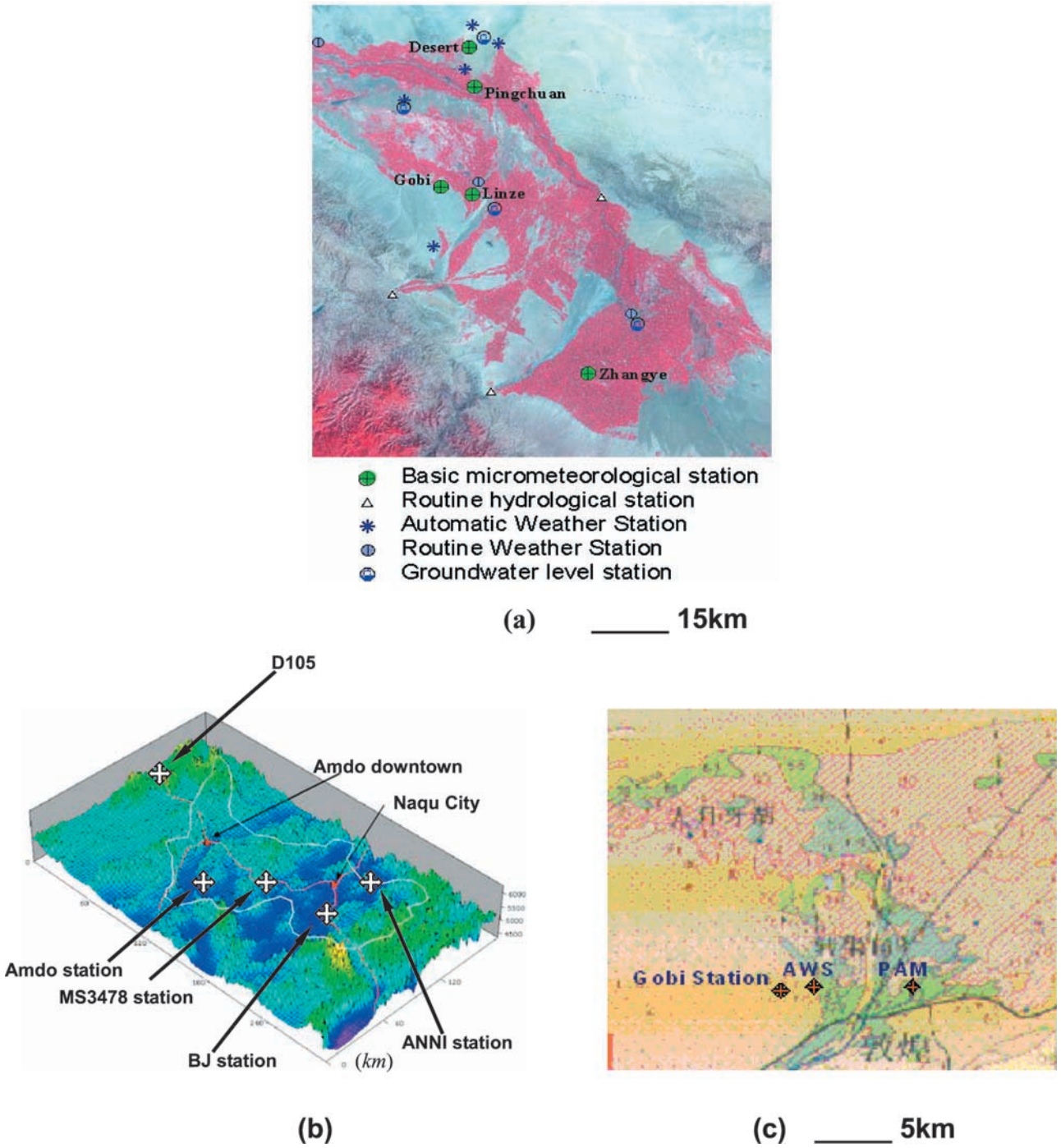

Figure 1. (a–c) The land surface condition and sites layout during the Heihe Basin Field Experiment (HEIFE), the Dun Huang Experiment (DHEX), and the Coordinated Enhanced Observing Period Asia-Australia Monsoon Project on the Tibetan Plateau (CAMP/Tibet). In Figure 1a, the red part is oasis or irrigated farm and the rest is the Gobi desert. In Figure 1c, the green and blue parts are oasis or irrigated farm and the rest is the Gobi desert. AWS is automatic weather station, and PAM is portable automated mesonet.

above) a height of about 300 m overlying the two very different land surfaces of the Gobi and the oasis. It means that u, T_a, and q have become well mixed at (and above) the height of about 300 m. In other words, the surface heterogeneity has no influence above 300, and this height can be regarded as a blending height z_b.

[14] 2. The vertical profiles of u, T_a, and q overlying the surfaces of the Gobi desert and the oasis (PAM station in Figure 1c) in the DHEX area are different in the near-surface layer owing to the different surface properties. The values of u and T_a below a height of about 150 m over the Gobi desert surface are higher than those over the oasis; q over the Gobi desert surface is lower than that over the oasis. The values of u, T_a, and q become almost the same at (and above) a height of about 150 m overlying the two very different land surfaces of the Gobi and the oasis. It means

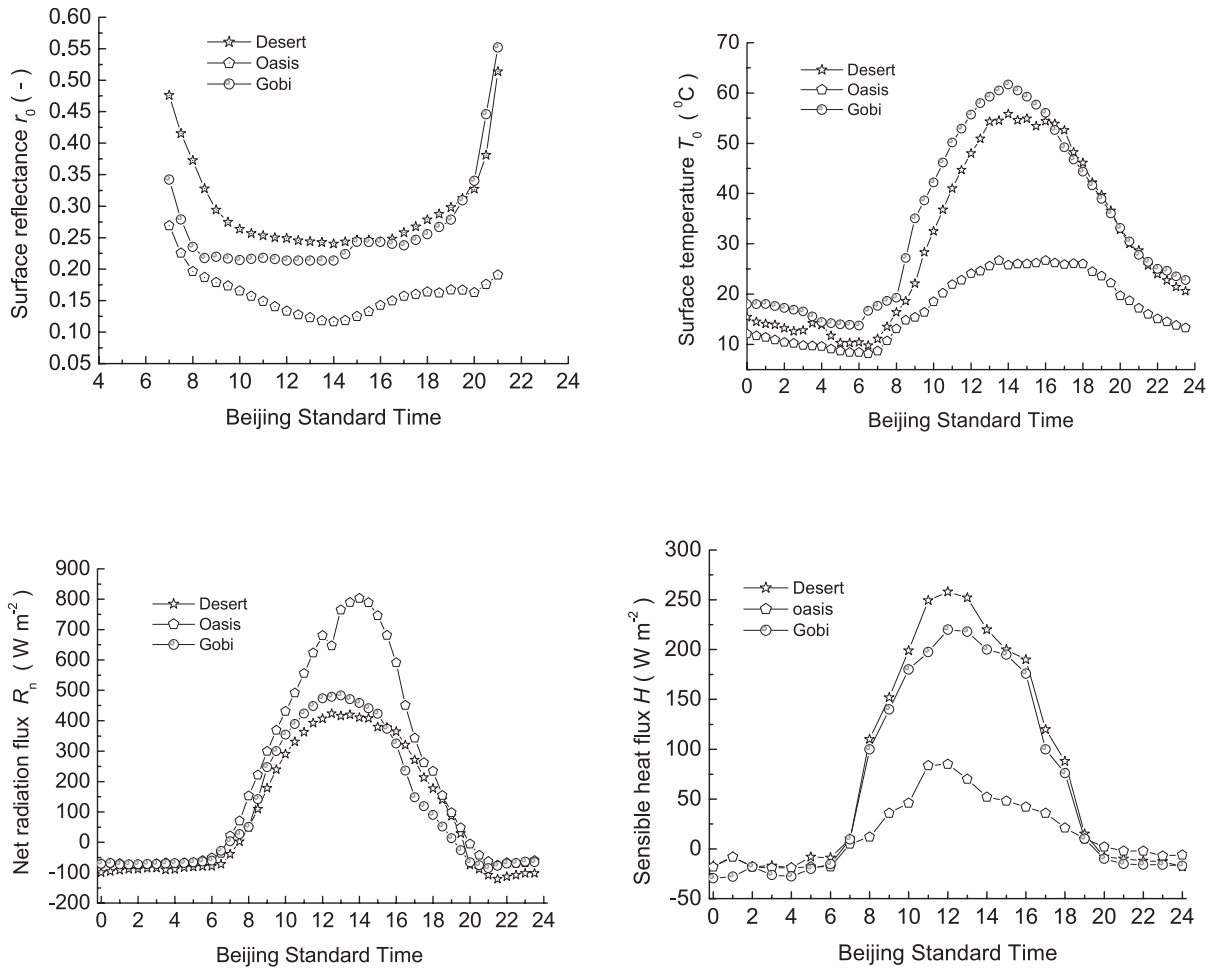

Figure 2. Comparisons of diurnal variations of surface reflectance r_0, surface temperature T_0, net radiation flux R_n, and sensible heat flux H on 9 July 1991 above desert, oasis, and Gobi surfaces obtained in the Heihe Basin Field Experiment (HEIFE) stations.

that the ABL variables have become well mixed above the height of about 150 m. It can also be seen very clearly that the blending height (150 m) over the DHEX area is lower than that over the HEIFE area. The reason is that the oasis spatial scale in the DHEX area is smaller than that in the HEIFE area [*Ma et al.*, 2002, 2003b] (Figure 1). Therefore the vertical structure of the airflow in the DHEX adjusted quickly to changes in the surface properties. The relation between vertical and horizontal scales was analyzed by *Raupach and Finnigan* [1995].

[15] 3. Although only one radiosonde system was set up in the CAMP/Tibet area, the variability of the profiles of u, T_a, and q overlying the grassland surface of the BJ station can also be seen clearly when we compare observations on 2 d under the different atmospheric conditions, that is, 17 and 25 August 2004. The day 17 August 2004 was a day of dry, stronger wind and lower humidity, and 25 August 2004 was a day of little wet, weaker wind and higher humidity. Wind speed u increases with height at 1200 (Beijing Standard Time, BST, 8 h earlier than universal time) on 2 d, and it becomes almost constant between 250 m and 550 m (u is about 4.5 m s^{-1} at 1200 on 17 August 2004 and u is about 1.8 m s^{-1} at 1200 on 25 August 2004). T_a decreases with height on both days. The q at 1200 on 17 August 2004 decreases with height in the near-surface atmospheric layer, and it becomes almost constant (about 2.9 g Kg^{-1}) between 250 m and 550 m. On the other hand, q at 1200 in 25 August 2004 increases with height in the near-surface layer (it was called ''inverse humidity''), and it becomes almost constant (about 7.2 g Kg^{-1}) between 250 m and 480 m. Therefore, the height of about 250 m can be regarded as a blending height z_b over the BJ station of the CAMP/Tibet area. The area of the experiment consists of typical pattern of very similar landscape units [*Ma et al.*, 2003a] (Figure 1). Each unit consists of a flat extensive area where the instrumented tower is located, surrounded by lower hills. The blending height derived at the BJ station can, therefore, be considered representative of the entire experimental area of CAMP/Tibet.

3. Aerodynamic and Thermodynamic Variables Over the Different Land Surfaces

[16] Land surface heterogeneity leads to different thermo-aerodynamic atmospheric parameters (z_{0m}, z_{0h} and kB^{-1}) of the surface layer. Methods for estimating these parameters and the results obtained will be described in this section.

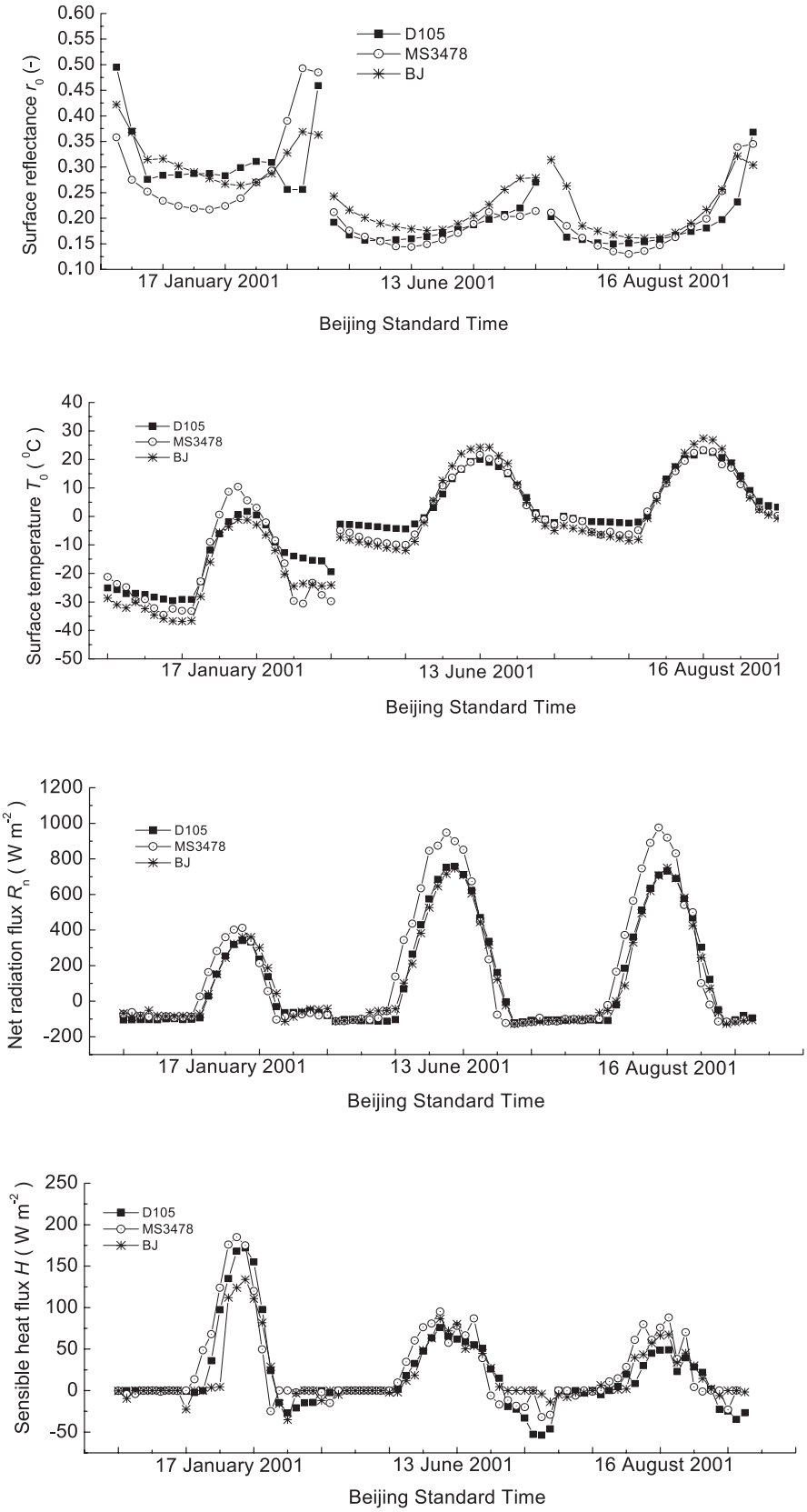

Figure 3. Comparisons of diurnal variations of surface reflectance r_0, surface temperature T_0, net radiation flux R_n, and sensible heat flux H over the CAMP/Tibet stations D105, MS3478, and BJ.

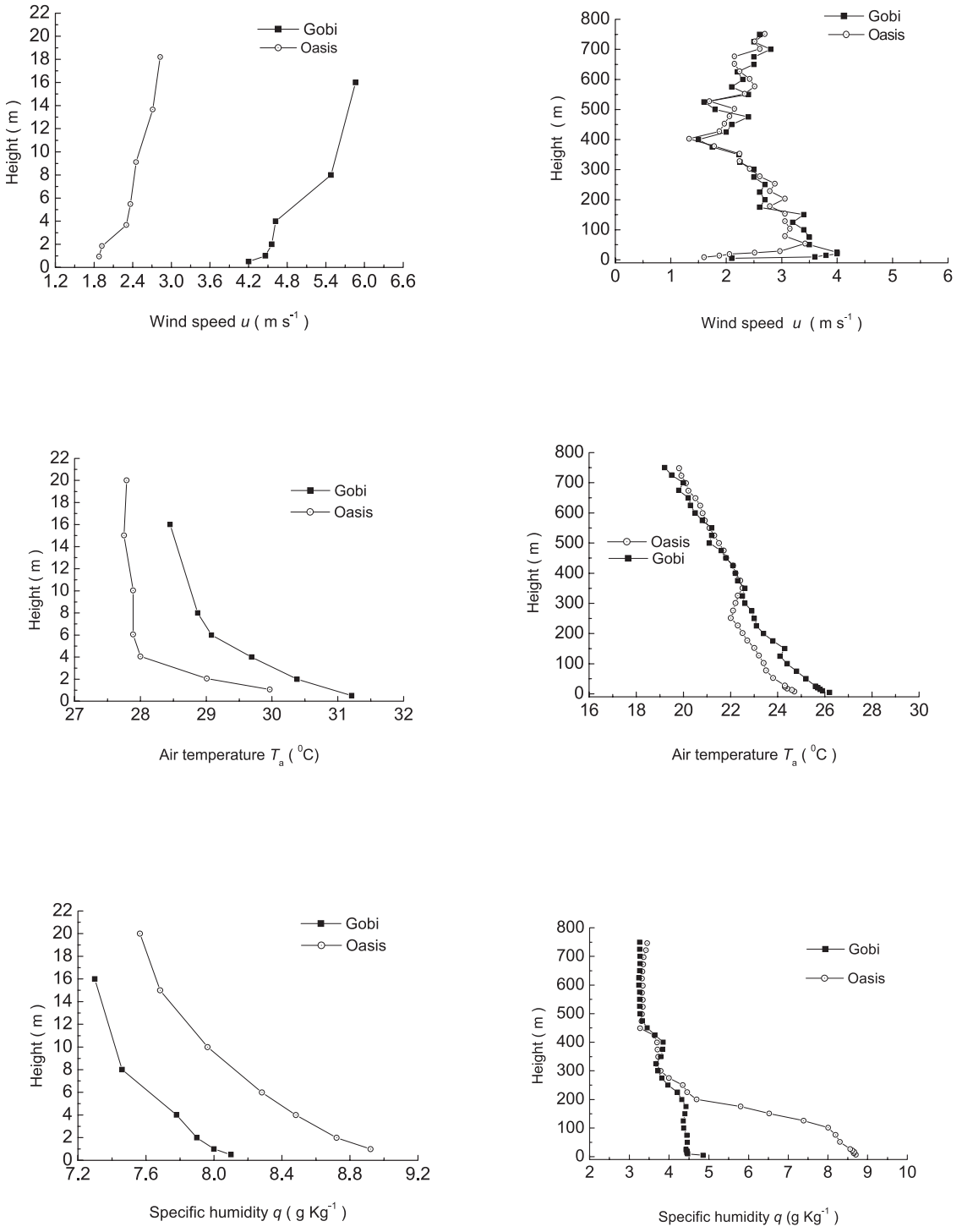

Figure 4. The profiles of horizontal wind speed u, air temperature T_a, and specific humidity q over the Gobi and the oasis of the Heihe Basin Field Experiment (HEIFE). (a) Data are from the atmospheric boundary layer (ABL) tower observations at 1200 Beijing Standard Time on 8 August 1991. (b) Data are from the tethered balloon observations at 1200 Beijing Standard Time on 15 August 1991.

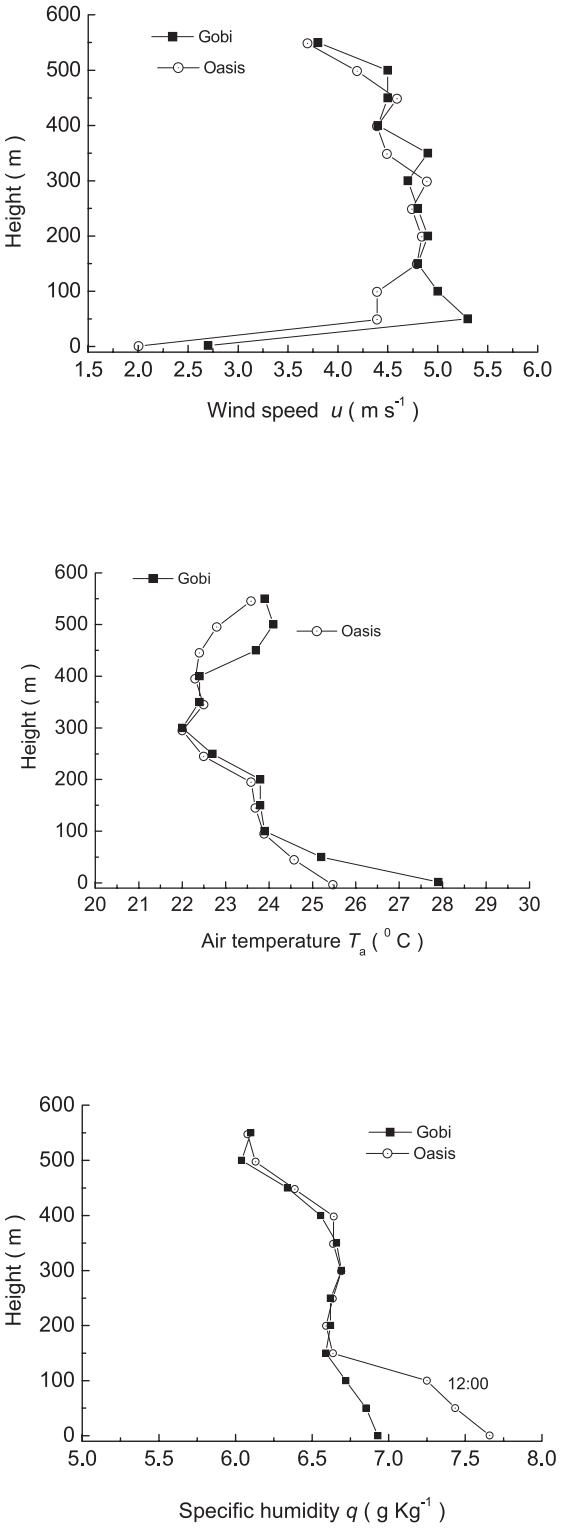

Figure 5. The profiles of horizontal wind speed u, air temperature T_a, and specific humidity q on 3 June 2002 over the Gobi desert and the oasis (PAM in Figure 1c) of the Dun Huang Experiment (DHEX).

3.1. Aerodynamic Roughness Length z_{0m}

[17] The aerodynamic roughness length for momentum, z_{0m}, can be derived using two methods, that is, the so-called independent method [*Chen et al.*, 1993] and the profile method.

3.1.1. Independent Method Using a Single Sonic Anemometer-Thermometer

[18] According to the Monin-Obukhov similarity theory [*Monin and Obukhov*, 1954], the gradient of nondimensional wind speed is written as

$$\frac{kz}{u*}\frac{\partial u}{\partial z} = \varphi_m\left(\frac{z}{L}\right) \quad (-). \tag{5}$$

Equation (5) is integrated to obtain the averaged wind speed U at height z as

$$U = \frac{u*}{k}\left[\ln\left(\frac{z}{z_{0m}}\right) - \psi_m\left(\frac{z}{L}\right)\right] \quad (\mathrm{ms}^{-1}), \tag{6}$$

where $\varphi_m\left(\frac{z}{L}\right)$ is the similarity universal function and $\psi_m\left(\frac{z}{L}\right)$ is the stability function of the wind profile, which becomes 0 under neutral conditions. The aerodynamic roughness length z_{0m} was derived from [*Chen et al.*, 1993]

$$z_{0m} = ze^{-\frac{kU}{u*}-\psi_m\left(\frac{z}{L}\right)} \quad (\mathrm{m}). \tag{7}$$

Through the same procedure the thermodynamic (heat transport) roughness length z_{0h} can be derived as

$$z_{0h} = ze^{-\frac{k(T_a-T_0)}{T_0}-\psi_h\left(\frac{z}{L}\right)} \quad (\mathrm{m}), \tag{8}$$

where $\psi_h\left(\frac{z}{L}\right)$ is the stability function of the temperature profile and $\psi_h\left(\frac{z}{L}\right) = 0$ under neutral conditions.

3.1.2. Profile Method

[19] When the atmosphere is under near-neutral conditions, equation (6) can be simplified to

$$U = \frac{u*}{k}\ln\left(\frac{z}{z_{0m}}\right) \quad (\mathrm{ms}^{-1}). \tag{9}$$

According to equation (9), if the averaged wind speed is observed at two different levels (z_1, z_2), the following expressions can be derived:

$$U_1 = \frac{u*}{k}\ln\left(\frac{z_1}{z_{0m}}\right) \quad (\mathrm{ms}^{-1}), \tag{10}$$

$$U_2 = \frac{u*}{k}\ln\left(\frac{z_2}{z_{0m}}\right) \quad (\mathrm{ms}^{-1}). \tag{11}$$

Finally, z_{0m} can be derived as

$$z_{0m} = e^{\left(\frac{U_2\ln z_1 - U_1\ln z_2}{U_2-U_1}\right)} \quad (\mathrm{m}). \tag{12}$$

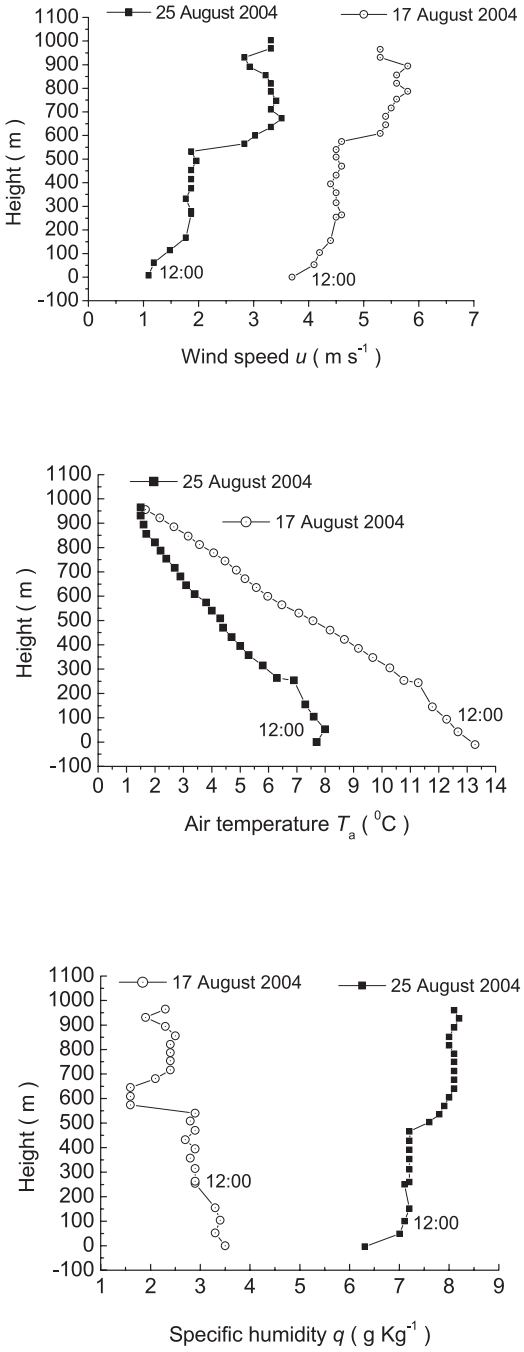

Figure 6. The profiles of horizontal wind speed u, air temperature T_a, and specific humidity q on 17 and 25 August 2004 at the BJ station in the Tibetan Plateau (CAMP/Tibet).

3.1.3. Results of z_{0m}

[20] Observations of the nondimensional wind speed kU/u_* versus the stability parameter $\zeta = z/L$ over the Amdo and NPAM stations of the GAME/Tibet are shown in Figures 7 and 9. Figure 8 shows the aerodynamic roughness length z_{0m} derived from the wind profile at the Amdo station. Using equations (7) and (12), the aerodynamic roughness length z_{0m} at the NPAM and Amdo stations in the GAME/Tibet area can be determined. The stability parameter $\zeta = z/L$ between -0.100 and 0.100 applies to

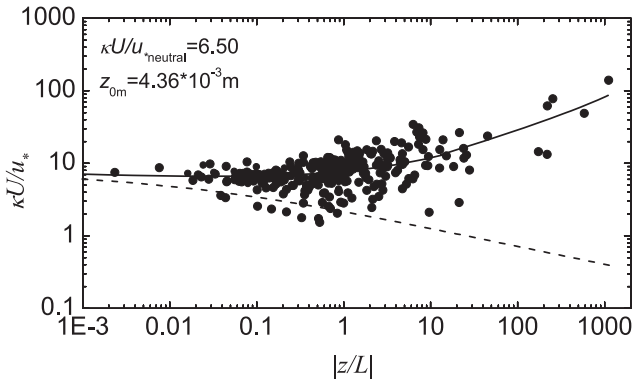

Figure 7. Nondimensional wind speed kU/u_* versus the stability parameter $\zeta = z/L$ as derived by the independent method over the Amdo station at the Tibetan Plateau (GAME/Tibet).

neutral conditions. The values of z_{0m} in the HEIFE and AECMP'95 areas were derived by the same method. All the results are shown in Table 1.

[21] The following can be seen from Figures 7–9 and Table 1: (1) z_{0m} is significantly different for grassland, sand desert, the Gobi, and the oasis (bean, wheat, and corn crop). (2) z_{0m} at the Amdo and NPAM stations of the GAME/Tibet is higher than the value obtained for Gobi and sand desert (HEIFE) but is lower than those obtained for the oasis (HEIFE: bean, wheat, and corn crop); z_{0m} at the NPAM station is larger than that at the Amdo station. (3) The values of z_{0m} obtained at the Amdo station with different methods (the results from the independent method in Figure 7 and the results from the profile method in Figure 8) are comparable. (4) z_{0m} at the NPAM station has a different value in different months (May, July, and August) owing to the high vegetation fractional cover in the station. The observation shows that the height of the grass at the NPAM station is about 5 cm in May, about 15 cm in July, and about 20 cm in August. It is clear that canopy height determines the aerodynamic roughness length z_{0m} at this station.

3.2. Thermodynamic Roughness Length z_{0h}

[22] Figure 10 shows the nondimensional air temperature $k(T_a - T_0)/T_*$ versus the stability parameter $\zeta = z/L$ at the

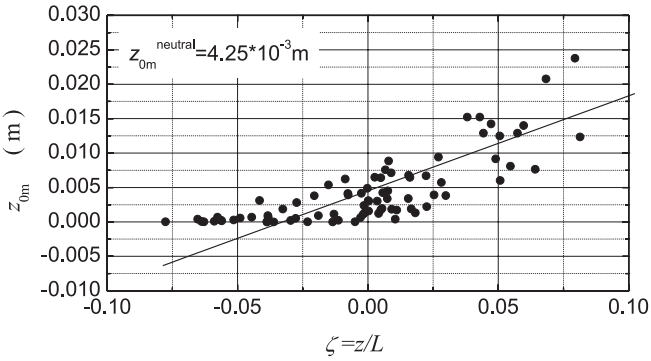

Figure 8. The surface momentum roughness length z_{0m} derived from the wind profile at the Amdo station in the Tibetan Plateau (GAME/Tibet).

Table 1. Aerodynamic Roughness Length z_{0m} Derived From Different Land Surfaces by Using the Independent Method

	Amdo	*NPAM*	*HEIFE*	*HEIFE*	*HEIFE*	*HEIFE*	*AECMP'95*
Land surface	grassland, ~5 cm	grassland, ~15 cm	sand desert	very sparse vegetation (Gobi)	bean, ~0.4 m	wheat, ~1.0 m	corn, ~1.8 m
Observation height, m	2.90	5.60	2.90	2.90	2.90	2.90	4.90
z_{0m}, m	0.00436 ± 0.00040	0.00564 (May), 0.0139 (July), 0.0324 (August)	0.00267 ± 0.0003	0.00280 ± 0.00030	0.06100 ± 0.00400	0.16800 ± 0.03000	0.30200 ± 0.0200

Amdo station in the Tibet Plateau. These observations yield $z_{0h\text{-}Amdo}$ = 0.000409 m with $\zeta = z/L$ between −0.100 and 0.100 applying to neutral conditions. The thermodynamic roughness length z_{0h} of grassland, sand desert, the Gobi, and the oasis are given in Table 2. They were obtained by the same method as mentioned in the previous section. It indicates that z_{0h} has very different values for different land cover types and z_{0h} is 1 order of magnitude smaller than z_{0m} in the GAME/Tibet area. The reason is that the thermodynamic roughness length z_{0h} is not only a function of temperature gradient, but is also affected by the canopy height and fractional vegetation cover.

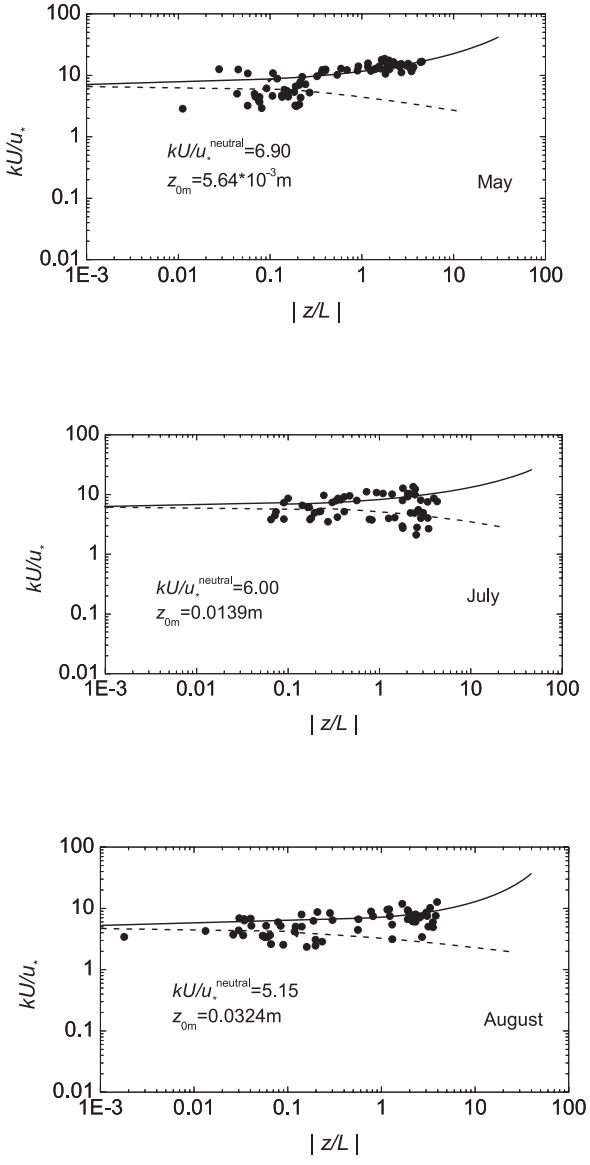

Figure 9. Nondimensional wind speed kU/u_* versus the stability parameter $\zeta = z/L$ at the NPAM (MS3478) station in the Tibetan Plateau (GAME/Tibet) in the months May, July, and August.

3.3. Excess Resistance to Heat Transfer kB^{-1}

[23] The excess resistance to heat transfer kB^{-1} is used to parameterize the sensible heat exchange between the land surface and atmosphere. It appears as a variable in many numerical models and satellite remote-sensing parameterization methods [*Su et al.*, 2001; *Su*, 2002; *Jia*, 2004] and can be derived from the following equation [*Owen and Thomson*, 1963; *Chamberlain*, 1968]:

$$kB^{-1} = \ln\left(\frac{z_{0m}}{z_{0h}}\right) \quad (-). \tag{13}$$

[24] An alternative expression for kB^{-1} can be obtained from the bulk transfer equation as [*Monteith*, 1973]

$$kB^{-1} = \frac{ku_*(T_0 - T_a)}{H_{obs}/\rho c_p} - \left[\ln\frac{z - d_0}{z_{0m}} - \psi_h\left(\frac{z}{L}\right)\right] \quad (-), \tag{14}$$

where u_*, H_{obs}, and L can be derived from the data observed by using a ABL tower and sonic anemometer-thermometer. On the basis of turbulent measurements and k = 0.40, z_{0m} was derived from equations (7) and (12); zero-plane displacement d_0 was obtained from $d_0 = (2/3)\, h_v$ [*Brutsaert*, 1984] for every station, with h_v being the canopy height. The kB^{-1} values derived from equation (13) for different land cover types are shown in Table 3.

[25] The following conclusions can be drawn:

[26] 1. kB^{-1} values are different on the different land surfaces. The reason was explained by *Su et al.* [2001], who made a detailed study on this issue.

[27] 2. The average values of $kB^{-1}{}_{NPAM}$ = 2.50 and $kB^{-1}{}_{Amdo}$ = 2.36 derived from equation (13) are very close to the results of $kB^{-1}{}_{NPAM}$ = 2.56 and $kB^{-1}{}_{Amdo}$ = 2.40 derived from equation (14). The latter two values were averaged over 10 observations from 900 A.M. Beijing Standard Time (BST) to 600 P.M. BST.

[28] 3. The averaged kB^{-1} of the GAME/Tibet area agree with the well-known result kB^{-1} = 2.3 [*Choudhury*, 1989], but it is larger than 2.3 in the areas of the HEIFE and the AECMP'95. Some values in Table 3 are almost the same as

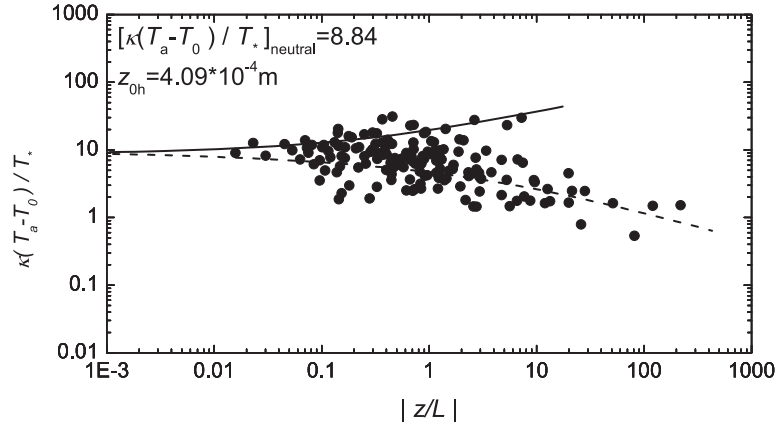

Figure 10. Nondimensional air temperature $k(T_a - T_0)/T_*$ versus the stability parameter $\zeta = z/L$ at the Amdo station in the Tibetan Plateau (GAME/Tibet).

the model results derived by *Su et al.* [2001], owing to the same land surface conditions.

4. Summary and Conclusions

[29] Understanding the surface layer (SL) and atmospheric boundary layer (ABL) processes over heterogeneous land surfaces is very important in the procedure of scaling up heat fluxes from the observational station, that is, ''point'' level to the regional scale. The land surface heterogeneity and its influences on the overlying atmospheric layer and the aerodynamic and thermodynamic parameters have been analyzed by using SL and ABL observations during the GAME/Tibet, the CAMP/Tibet, the HEIFE, the DHEX, and the AECMP'95. The results described in this paper can be summarized as follows:

[30] 1. Very different values of surface reflectance r_0, surface temperature T_0, net radiation flux R_n, and sensible heat flux H between the Gobi desert and the oasis show that land surface heterogeneity is very significant in the HEIFE area. Surface heterogeneity at the CAMP/Tibet area is less significant than that in the HEIFE area.

[31] 2. The land surface heterogeneity leads in the near-surface layer to different vertical profiles of horizontal wind speed u, air temperature T_a, and specific humidity q overlying the surfaces of the Gobi and the oasis in the areas of the HEIFE and DHEX. The values of u, T_a, and q become well mixed above a height of about 300 m at the HEIFE and 150 m at the DHEX. It means that a clearly defined blending height z_b can be observed over both experimental areas. The difference of z_b results from the different oasis horizontal scale of heterogeneity and the different wind speed [*Mason*, 1988]. In other words, the larger oasis scale will lead to a higher z_b value. Although only one radiosonde system data were available, on a normal summer day about 250 m can be regarded as a blending height over the whole CAMP/Tibet area. It is also very clear that z_b determined by the ABL observations over the experimental areas is a direct and correct way.

[32] 3. The aerodynamic roughness length z_{0m} and the thermodynamic roughness length z_{0h} are significantly different over the different land surfaces of grassland, the Gobi, sand desert, and the oasis. For the GAME/Tibet area, z_{0h} is one magnitude smaller than z_{0m}. It means that both the aerodynamic and thermodynamic characteristics of the land surface have effects on z_{0m} and z_{0h}.

[33] 4. The excess resistance to heat transfer, kB^{-1}, has obvious characteristics over different land cover types. It has different values for grassland, the Gobi, sand desert, and the oasis. It is very clear that a kB^{-1}-value of 2.3 cannot be used as a general value for the areas of the HEIFE and the AECMP'95.

[34] Additional general conclusions that can be drawn are the following:

[35] 1. Very different land cover types and hydrological conditions (e.g., the oasis and the Gobi desert over the HEIFE area and the DHEX area) lead to different vertical structures in the surface layer (SL) and atmospheric boundary layer (ABL). These layers, however, adjust to land surface properties over spatial scales varying from 1 to 10 km. It means that different ABL vertical profiles and different resistances exist near the land surface over quite different land surfaces.

[36] 2. Limited land surface heterogeneities such as the grassland and topography over the areas of the GAME/Tibet and the CAMP/Tibet, results, however, in the same SL and

Table 2. Thermodynamic Roughness Length z_{0h} Derived From Different Land Surfaces

	Amdo	*NPAM*	*HEIFE*	*HEIFE*	*HEIFE*	*HEIFE*	*AECMP'95*
Land surface	grassland, ~5 cm	grassland, ~15 cm	sand desert	very sparse vegetation (Gobi)	bean, ~0.4 m	wheat, ~1.0 m	corn, ~1.8 m
Height of observation, m	2.90	5.60	2.90	2.90	2.90	2.90	4.90
z_{0h}, m	0.00041 ± 0.00005	0.00051 (May), 0.00114 (July), 0.00231 (August)	0.000049	0.000011	0.000685	0.00132	0.00227

Table 3. Excess Resistance to Heat Transfer kB^{-1} of Different Land Cover Types

	Amdo	*NPAM*	*HEIFE*	*HEIFE*	*HEIFE*	*HEIFE*	*AECMP'95*
Land surface	grassland ~5 cm	grassland ~15 cm	sand desert	very sparse vegetation (Gobi)	bean ~0.4 m	wheat ~1.0 m	corn ~1.8 m
Observed height, m	2.90	5.60	2.90	2.90	2.90	2.90	4.90
$\overline{kB^{-1}}$	2.36	2.50	4.00	5.50	4.49	4.85	4.89

ABL over the whole area. In other words, in these areas the land surface is statistically homogeneous and the ABL adjusts to a mixture combination of small-scale heterogeneities. Therefore, effective variables and one resistance may for such conditions be used to determine the sensible and latent heat fluxes.

[37] The above mentioned concepts, as well as the aerodynamic and thermodynamic parameters determined in this paper, may further be used to parameterize the near-surface heat fluxes used in addition to satellite measurements.

[38] **Acknowledgments.** This work was completed under the auspices of the Chinese National Key Programme for Developing Basic Sciences (2005CB422003), National Natural Science Foundation of China (40675012), and the Innovation Project of Chinese Academy of Sciences (KZCX3-SW-231). Most parts of this study were done as cooperative research works in Alterra, Wageningen University and Research Center (WUR), Netherlands (supported by the EC FP6 GMES EAGLE project, contract 502057), and the International Institute for Geo-Information Science and Earth Observation (ITC), Netherlands. The authors thank all the participants from China and Japan in the field observations of the HEIFE, the AECMP'95, the GAME/Tibet, and the CAMP/Tibet.

References

Brutsaert, W. (1984), *Evaporation Into the Atmosphere: Theory, History, and Applications*, 299 pp., Springer, New York.

Chamberlain, A. C. (1968), Transport of gases to and from surfaces with bluff and wave-like roughness elements, *Q. J. R. Meteorol. Soc.*, *94*, 318–332.

Chen, J., J. Wang, and Y. Mitsuta (1993), An independent method to determine the surface roughness length (in Chinese with English abstract), *Chin. J. Atmos. Sci.*, *17*(1), 21–26.

Choudhury, B. J. (1989), Estimating evaporation and carbon assimilation using infrared temperature data: Vistas in modeling, in *Theory and Application of Optical Remote Sensing*, edited by G. Asrar, pp. 628–690, John Wiley, New York.

Claussen, M. (1990), Area-averaging of surface fluxes in a neutrally stratified, horizontally inhomogeneous atmospheric boundary layer, *Atmos. Environ.*, *24*, 1349–1360.

Claussen, M. (1991), Estimation of areally averaged surface fluxes, *Boundary Layer Meteorol.*, *54*, 387–410.

Jia, L. (2004), Modeling heat exchanges at land-atmosphere interface using multi-angular thermal infrared measurements, Ph.D. thesis, 199 pp., Wageningen Univ., Netherlands.

Ma, Y., O. Tsukamoto, H. Ishikawa, Z. Su, M. Menenti, J. Wang, and J. Wen (2002), Determination of regional land surface heat flux densities over heterogeneous landscape of HEIFE integrating satellite remote sensing with field observations, *J. Meteorol. Soc. Jpn.*, *80*(3), 485–501.

Ma, Y., Z. Su, T. Koike, T. Yao, H. Ishikawa, K. Ueno, and M. Menenti (2003a), On measuring and remote sensing surface energy partitioning over the Tibetan Plateau: From GAME/Tibet to CAMP/Tibet, *Phys. Chem. Earth*, *28*, 63–74.

Ma, Y., J. Wang, R. Huang, G. Wei, M. Menenti, Z. Su, Z. Hu, F. Gao, and J. Wen (2003b), Remote sensing parameterization of land surface heat fluxes over arid and semi-arid areas, *Adv. Atmos. Sci.*, *20*(4), 530–539.

Ma, Y., M. Menenti, O. Tsukamoto, H. Ishikawa, J. Wang, and Q. Gao (2004), Remote sensing parameterization of regional land surface heat fluxes over arid area in northwestern China, *J. Arid Environ.*, *57*, 117–133.

Mason, P. (1988), The formation of areally averaged roughness lengths, *Q. J. R. Meteorol. Soc.*, *114*, 399–420.

Monin, A. S., and A. M. Obukhov (1954), Basic laws of turbulent mixing the atmospheric near the ground, *Tr. Akad. Nauk. SSSR., Geofiz. Inst.*, *24*(151), 163–187.

Monteith, J. I. (1973), *Principles of Environmental Physics*, 241 pp., Edward Arnold, London.

Owen, P. R., and W. R. Thomson (1963), Heat transfer across rough surfaces, *J. Fluid Mech.*, *15*, 321–334.

Raupach, M. R., and J. J. Finnigan (1995), Scale issues in boundary-layer meteorology: Surface energy balances in heterogeneous terrain, *Hydrol. Processes*, *9*, 589–612.

Su, Z. (2002), The Surface Energy Balance System (SEBS) for estimation of turbulent heat fluxes, *Hydrol. Earth Syst. Sci.*, *6*, 85–99.

Su, Z., T. Schmugge, W. P. Kustas, and W. J. Massman (2001), An evaluation of two models for estimation of the roughness height for heat transfer between the land surface and the atmosphere, *J. Appl. Meteorol.*, *40*, 1933–1951.

Wieringa, J. (1986), Roughness-dependent geographical interpolation of surface wind speed averages, *Q. J. R. Meteorol. Soc.*, *112*, 867–889.

R. Feddes, Department of Environmental Sciences, Wageningen University, NL-6700 HB Wageningen, Netherlands.

Y. Ma, Institute of Tibetan Plateau Research, Chinese Academy of Sciences, 18 Shuangqing Road, Haidian District, P.O. Box 2871, Beijing 100085, China. (ymma@itpcas.ac.cn)

M. Menenti, Laboratoire des Sciences de l'Image, de l'Informatique et de la Télédétection, Université Louis Pasteur, F-67400 Strasbourg, France.

J. Wang, Cold and Arid Regions Environmental and Engineering Research Institute, Chinese Academy of Sciences, Lanzhou 730000, China.